

PAPER • OPEN ACCESS

Locomotion performance for oscillatory swimming in free mode

To cite this article: D Paniccia *et al* 2023 *Bioinspir. Biomim.* **18** 015004

View the [article online](#) for updates and enhancements.

You may also like

- [A dual caudal-fin miniature robotic fish with an integrated oscillation and jet propulsive mechanism](#)
Pan Liao, Shiwu Zhang and Dong Sun
- [Fin–fin interactions during locomotion in a simplified biomimetic fish model](#)
David G Matthews and George V Lauder
- [Computational modeling of swimming in marine invertebrates with implications for soft swimming robots](#)
Zhuoyu Zhou and Rajat Mittal



Bioinspiration & Biomimetics



PAPER

Locomotion performance for oscillatory swimming in free mode

OPEN ACCESS

D Paniccia* , L Padovani, G Graziani  and R Piva

Department of Mechanical and Aerospace Engineering, Sapienza University, Rome, Italy

* Author to whom any correspondence should be addressed.

E-mail: damiano.paniccia@uniroma1.it

RECEIVED
3 June 2022

REVISED
24 October 2022

ACCEPTED FOR PUBLICATION
1 November 2022

PUBLISHED
18 November 2022

Keywords: oscillatory swimming, fish locomotion, recoil reactions, free swimming mode, flapping foil

Supplementary material for this article is available [online](#)

Original Content from this work may be used under the terms of the [Creative Commons Attribution 4.0 licence](#).

Any further distribution of this work must maintain attribution to the author(s) and the title of the work, journal citation and DOI.



Abstract

Oscillatory swimming of a fishlike body, whose motion is essentially promoted by the flapping tail, has been studied almost exclusively in axial mode under an incoming uniform stream or, more recently, self-propelled under a virtual body resistance. Obviously, both approaches do not consider the unavoidable recoil motions of the real body which have to be necessarily accounted for in a design procedure for technological means. Actually, once combined with the prescribed kinematics of the tail, the recoil motions lead to a remarkable improvement on the resulting swimming performance. An inviscid impulse model, linear in both potential and vortical contributions, is a proper tool to obtain a deeper comprehension of the physical events with respect to more elaborated flow interaction models. In fact, at a first look, the numerical results seem to be quite entangled, since their trends in terms of the main flapping parameters are not easy to be identified and a fair interpretation is obtained by means of the model capability to separate the effects of added mass and vortex shedding. Specifically, a prevailing dependence of the potential contribution on the heave amplitude and of the vortical contribution on the pitch amplitude is instrumental to unravel their combined action. A further aid for a proper interpretation of the data is provided by accounting separately for a geometrical component of the recoil which is expected to follow from the annihilation of any spurious rigid motion in case no fluid interactions occur. The above detailed decomposition of the recoil motions shows, through the numerical results, how the single components are going to influence the main flapping parameters and the locomotion performance as a guide for the design of biomimetic swimmers.

1. Introduction

Several fish species, like tunafish, are assumed to produce their locomotion almost exclusively by oscillating their caudal fin while the rest of the body should essentially contribute to both inertial and viscous resistance. The performance of these oscillatory swimmers has been usually evaluated by the Froude efficiency of the flapping foil propulsor, with assigned heave and pitch motions, under a prescribed uniform stream [1–6] or by the cost of transport for the whole body, consisting of a flapping foil plus a resistant virtual body, self-propelled in axial mode [7, 8]. A comparative analysis of the above two parameters for evaluating the swimming performance has been deeply analyzed to prove their suitability for different swimming gaits [9, 10]. The above

procedures are both very convenient for experimental and numerical investigations, but unable to account for the actual motion of the fishlike body in free swimming mode and for its presumed impact on the overall performance [11–14]. In fact, as firmly stated by Lighthill [15], the locomotion is necessarily accompanied by some recoil motions whose effect has to be accounted for to satisfy the equilibrium equations. The recoil velocity components have been shown to modify, for undulatory swimming, the resulting kinematics to reach a favorable effect on the overall efficiency while for constrained or tethered cases, where their influence is neglected, different results are obtained for both locomotion speed and expended energy so to experience a poorer swimming performance [16–20]. The focus of the present work is on the analysis of the recoil motions for oscillatory

swimming with the purpose to find whether they play a similar role also in this case. In fact, the deformation is now essentially limited to the rear end of the body and one could expect rather small recoil reactions with a presumably low impact on the overall performance [21]. In spite of this common belief, we claim here that the recoil induced modifications of the flapping tail parameters cannot be neglected and even more they produce an overall improvement of the swimming performance. For a better comprehension of these large scale effects, we intend, as a proper way, to analyze separately the different components of the recoil motions and their influence on the fish dynamics. Specifically, the potential and vortical contributions given by the interaction with the surrounding fluid and the geometrical component of the recoil which instead is an *a priori* requirement to satisfy the equilibrium of the fishlike body for any given deformation.

The reported numerical results are obtained by a simple impulse model which is able to isolate the added mass and the vortex-shedding contributions without using more elaborated simulations which might obscure the essence of the problem. A detailed analysis of the inviscid results for different values of the prescribed kinematic parameters is instrumental to devise the influence of the recoil motion for a suitable design procedure of free swimming biomimetic means.

2. Materials and methods

2.1. Mathematical model

The self-propelled motion of an impermeable, flexible body \mathcal{B} with bounding surface $\partial\mathcal{B}$ is modeled by assuming a two-dimensional incompressible flow in an unbounded fluid domain \mathcal{V} with density ρ . Only internal actions are exchanged between the swimming body and the surrounding fluid, whose velocity vanishes at the far field boundary.

By adopting the impulse formulation (see e.g. [22–24]) for both linear and angular fluid momenta and assuming \mathbf{n} as the normal to $\partial\mathcal{B}$ pointing into the fluid domain \mathcal{V} , the force \mathbf{F}_b and the moment \mathbf{M}_b acting on the body are obtained as the time derivatives of the linear impulse, \mathbf{p} , and angular impulse, $\boldsymbol{\pi}$:

$$\begin{aligned} \mathbf{F}_b &= -\frac{d\mathbf{p}}{dt} \\ &= -\frac{d}{dt} \left[\int_{\mathcal{V}} \rho \mathbf{x} \times \boldsymbol{\omega} dV + \int_{\partial\mathcal{B}} \rho \mathbf{x} \times (\mathbf{n} \times \mathbf{u}) dS \right] \\ \mathbf{M}_b &= -\frac{d\boldsymbol{\pi}}{dt} \\ &= \frac{d}{dt} \frac{1}{2} \left[\int_{\mathcal{V}} \rho |\mathbf{x}|^2 \boldsymbol{\omega} dV + \int_{\partial\mathcal{B}} \rho |\mathbf{x}|^2 (\mathbf{n} \times \mathbf{u}) dS \right] \end{aligned} \quad (1)$$

where $\boldsymbol{\omega}$ is the vorticity and \mathbf{u} stays for the limiting value of the fluid velocity on $\partial\mathcal{B}$.

The fluid velocity field is expressed through a Helmholtz decomposition as

$$\mathbf{u} = \nabla\phi + \nabla \times \boldsymbol{\Psi} = \nabla\phi + \mathbf{u}_w \quad (2)$$

where the scalar potential ϕ and the (solenoidal) vector potential $\boldsymbol{\Psi}$ are easily obtained by imposing the impermeable boundary condition on $\partial\mathcal{B}$ and vanishing velocity at infinity. According to this decomposition, we express the linear impulse \mathbf{p} in terms of its potential and vortical contributions as $\mathbf{p} = \mathbf{p}_\phi + \mathbf{p}_v$, where the potential impulse \mathbf{p}_ϕ and the vortical impulse \mathbf{p}_v are given by (see [25] for further details)

$$\begin{aligned} \mathbf{p}_\phi &= -\rho \int_{\partial\mathcal{B}} \phi \mathbf{n} dS \\ \mathbf{p}_v &= \int_{\mathcal{V}} \rho \mathbf{x} \times \boldsymbol{\omega} dV + \int_{\partial\mathcal{B}} \rho \mathbf{x} \times (\mathbf{n} \times \mathbf{u}_w) dS. \end{aligned} \quad (3)$$

The same decomposition may be used for the angular impulse which, by using appropriate vector identities, can be split into its potential and vortical parts as $\boldsymbol{\pi} = \boldsymbol{\pi}_\phi + \boldsymbol{\pi}_v$, where

$$\begin{aligned} \boldsymbol{\pi}_\phi &= -\rho \int_{\partial\mathcal{B}} \mathbf{x} \times \phi \mathbf{n} dS \\ \boldsymbol{\pi}_v &= -\frac{1}{2} \int_{\mathcal{V}} \rho |\mathbf{x}|^2 \boldsymbol{\omega} dV \\ &\quad - \frac{1}{2} \int_{\partial\mathcal{B}} \rho |\mathbf{x}|^2 (\mathbf{n} \times \mathbf{u}_w) dS. \end{aligned} \quad (4)$$

By combining the Newton laws with equation (1) and by eliminating the time derivatives, we obtain, for null initial conditions, the conservation of the linear and angular momenta as

$$\begin{aligned} \int_{\mathcal{B}} \rho_b \mathbf{u}_b dV + \mathbf{p} &= 0 \\ \int_{\mathcal{B}} \rho_b \mathbf{x} \times \mathbf{u}_b dV + \boldsymbol{\pi} &= 0. \end{aligned} \quad (5)$$

The body velocity \mathbf{u}_b is given by the sum of the prescribed deformation velocity \mathbf{u}_{sh} plus the unknown rigid motion of the body-fixed frame with origin in the centre-of-mass (translational, \mathbf{u}_{cm} , and rotational, $\boldsymbol{\Omega}$, velocity):

$$\mathbf{u}_b = \mathbf{u}_{sh} + \mathbf{u}_{cm} + \boldsymbol{\Omega} \times \mathbf{x}' \quad (6)$$

where \mathbf{x}' is the position vector in the body frame, i.e. $\mathbf{x} = \mathbf{x}_{cm} + \mathbf{x}'$.

As a mandatory requirement for equation (6) to be valid, since no rigid motions are allowed for an isolated body, the body deformation velocity have to satisfy the following two conditions

$$\int_{\mathcal{B}} \rho_b \mathbf{u}_{sh} dV = 0 \quad \int_{\mathcal{B}} \rho_b \mathbf{x}' \times \mathbf{u}_{sh} dV = 0 \quad (7)$$

so as the net linear and angular momenta of the imposed kinematics are equal to zero. Finally, by

combining equations (5) and (6) with the above conditions (7), we obtain:

$$\begin{aligned} m_b \mathbf{u}_{cm} + \mathbf{p} &= 0 \\ I_{zz} \Omega + \pi' &= 0 \end{aligned} \quad (8)$$

where the angular impulse is recast in terms of the distance \mathbf{x}' as $\pi' = (\boldsymbol{\pi} - \mathbf{x}_{cm} \times \mathbf{p}) \cdot \mathbf{e}_3$ and $\mathbf{x}_{cm} = x_{cm} \mathbf{e}_1 + y_{cm} \mathbf{e}_2$ is the position of the body center of mass.

In the most general case, especially when designing a prescribed deformation kinematics $\bar{\mathbf{u}}_{sh}$, equation (7) are very unlikely to be satisfied and they read as

$$\int_{\mathcal{B}} \rho_b \bar{\mathbf{u}}_{sh} dV = m_b \mathbf{u}_0 \quad \int_{\mathcal{B}} \rho_b \mathbf{x}' \times \bar{\mathbf{u}}_{sh} dV = I_{zz} \Omega_0 \quad (9)$$

where m_b and I_{zz} are the mass and the moment of inertia of the body respectively and \mathbf{u}_0 and Ω_0 represent spurious rigid motion embedded in the prescribed kinematics. In the present approach, to obtain directly the velocity of the body center of mass [26, 27], $\bar{\mathbf{u}}_{sh}$ should be properly modified by accounting for a corrective motion able to counterbalance and to annihilate \mathbf{u}_0 and Ω_0 . We refer to this motion as geometrical recoil correction, essential to ensure that any deformation assigned to the body is actually viable in the absence of the interactions with the surrounding fluid.

The expended energy is obtained in terms of the fluid kinetic energy released into the flow field [28] as

$$\begin{aligned} E &= \frac{1}{2} \int_S \phi \frac{\partial \phi}{\partial n} dS + \frac{1}{2} \int_S (\mathbf{u}_w \times \boldsymbol{\psi}) \cdot \mathbf{n} dS \\ &+ \frac{1}{2} \int_V \boldsymbol{\psi} \cdot \boldsymbol{\omega} dV \end{aligned} \quad (10)$$

where the last term is commonly known as the excess energy while the first two integrals are usually quite negligible at steady state conditions.

2.2. Solution procedure

Going back to the Helmholtz decomposition introduced by equation (2), the scalar potential may be further divided as $\phi = \phi_{sh} + \phi_{loc}$ [29], so as

$$\frac{\partial \phi_{sh}}{\partial n} = \mathbf{u}_{sh} \cdot \mathbf{n} \quad \frac{\partial \phi_{loc}}{\partial n} = (\mathbf{u}_{cm} + \boldsymbol{\Omega} \times \mathbf{x}') \cdot \mathbf{n} \quad (11)$$

where ϕ_{sh} and ϕ_{loc} are associated to the prescribed deformation velocity \mathbf{u}_{sh} and to the locomotion (linear and angular) velocity respectively, according to the related boundary conditions on S_b . It follows that the linear and angular impulses may be also split as

$$\mathbf{p}_\phi = \mathbf{p}_{sh} + \mathbf{p}_{loc} \quad \pi'_\phi = \pi'_{sh} + \pi'_{loc} \quad (12)$$

accordingly with the above decomposition.

In line with classical treatises (see e.g. [30]), we may express \mathbf{p}_{loc} and π'_{loc} by defining the added mass coefficients m_{ij} as

$$m_{ij} = -\rho \int_{\partial \mathcal{B}} \Phi_i \frac{\partial \Phi_j}{\partial n} dS \quad (13)$$

where the Kirchhoff base potentials Φ_j are defined through the boundary conditions

$$\frac{\partial \Phi_1}{\partial n} = \mathbf{n} \cdot \mathbf{e}_1 \quad \frac{\partial \Phi_2}{\partial n} = \mathbf{n} \cdot \mathbf{e}_2 \quad \frac{\partial \Phi_3}{\partial n} = \mathbf{x}' \times \mathbf{n} \cdot \mathbf{e}_3 \quad (14)$$

to finally have

$$\phi_{loc} = \dot{x}_{cm} \Phi_1 + \dot{y}_{cm} \Phi_2 + \Omega \Phi_3. \quad (15)$$

By using equations (12) and (15), the final system of equations is obtained by recasting equation (8) in a reference frame fixed to the body center of mass. With the use of capital letters for the unknowns linear (V_1, V_2) and angular (Ω) velocities in this frame, we may bring to the right hand side only the known terms due to shape deformation and released vorticity, so to obtain the system

$$\begin{cases} V_1 (m_{11} + m_b) + V_2 m_{12} + \Omega m_{13} = -P_{sh1} - P_{v1} \\ V_1 m_{21} + V_2 (m_{22} + m_b) + \Omega m_{23} = -P_{sh2} - P_{v2} \\ V_1 m_{31} + V_2 m_{32} + \Omega (m_{33} + I_{zz}) = -\Pi_{sh} - \Pi_v \end{cases} \quad (16)$$

to be solved at each time step for the unknown velocity components. In the previous sections, to lighten the reading, the velocity components have been renamed as $U = -V_1$ and $V = V_2$, while the mean steady-state value of the forward velocity U will be referred to as the locomotion velocity U_{loc} which identifies the locomotion frame of reference, i.e. a reference frame moving with the locomotion velocity itself. The remaining lateral and angular velocity components V and Ω together with the forward velocity fluctuations U' , define the body-fixed frame motion within the locomotion frame and will be referred to as fluid recoil motions. Many authors (see e.g. [17, 18, 31]), by following Lighthill's first definition of recoil [32] as the motion to be added to a prescribed deformation to satisfy the linear and angular momentum conservation laws, do not distinguish between the geometrical recoil correction and the one resulting only from the fluid-body interaction, i.e. the fluid recoil. Although this approach substantially differs from the one proposed here, it is equally suitable to obtain the correct solution [26]. However, we favour our methodology since it is able to reveal the role of both contributions and may provide a useful insight for the design of optimal deformation gaits.

Finally, due to the linearity of the present model, the system of equation (16) is solved by splitting the unknown velocity components (U, V, Ω) into their potential contributions ($U_\phi, V_\phi, \Omega_\phi$) and their vortical contributions (U_v, V_v, Ω_v). The potential ones

are obtained by solving the system only for the potential impulses associated to the shape deformation \mathbf{P}_{sh} and Π_{sh} , while the vortical contributions are obtained by solving for the vortical impulses \mathbf{P}_v and Π_v .

The flow solutions are obtained by a simple 2D inviscid model with concentrated vorticity, which allow for neat and physically intuitive results. Specifically, we used an unsteady potential code based on the Hess and Smith approach [33], while the vortex shedding is treated by following the procedure described in [34]. This well-known numerical procedure has been extensively used in the literature to study rigid bodies like airfoils moving with a fully prescribed motion [2, 4, 35–37]. Since in the present application the linear and angular rigid body velocities are unknown for free swimming of a deformable body (see also [11, 12]), the coupling between its dynamics and the flow solution implies a much larger complexity.

2.3. Caudal fin shape and kinematics

The anterior part of the two-dimensional body is represented by a NACA0012 hydrofoil with length l_b while the caudal fin is represented by a NACA0004 with length l_t . The tail length l_t , illustrated in figure 1, is equal to 1/7 of the total body length $L = l_b + l_t$, as frequently observed in nature for oscillatory swimmers like tuna.

The caudal fin kinematics is fully prescribed and its flapping motion is given by the combination of a heaving motion of the peduncle $y_p(t)$ and a pitching motion about the peduncle itself given by $\theta(t)$. The pitch motion $\theta(t)$ has a phase angle $\phi = -\pi/2$ with respect to the heave motion, so to have

$$\begin{aligned} y_p(t) &= h_0 \sin(2\pi ft) \\ \theta(t) &= \theta_0 \sin(2\pi ft + \phi) \end{aligned} \quad (17)$$

where h_0 is the maximum heave amplitude, θ_0 is the maximum pitch angle and f is the oscillation frequency. The phase shift ϕ between these motions has been chosen to be consistent with many observations either in nature or in experimental investigations. According to these assumptions, the lateral motion of the caudal fin is finally given as

$$y_f(s_f, t) = y_p(t) - s_f \sin(\theta(t)) \quad (18)$$

where s_f goes from 0 to l_t , i.e. from the peduncle to the trailing edge of the tail, and $\theta(t)$ is taken positive in the clockwise direction.

With regard to the prescribed body deformation, we followed a path similar to the one suggested by Li *et al* [38] for a pure oscillation of the rear-end of the anterior body, but we consider a proper undulatory motion to better represent the shape deformations observed in real fish. The procedure to obtain the body kinematics, which is both fitting the flapping motion of the caudal fin and satisfying the inextensibility condition, is described in the [appendix](#).

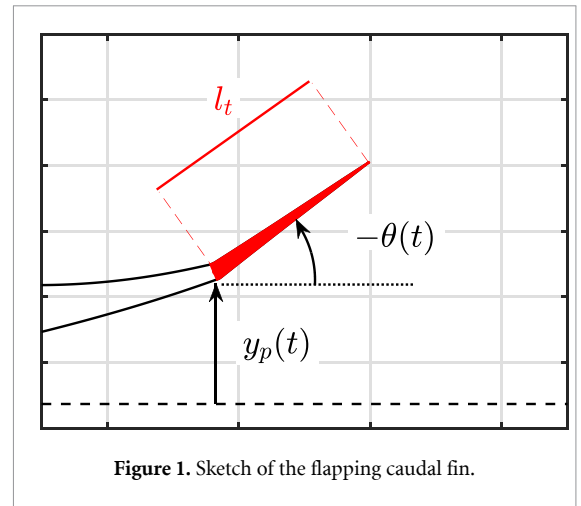


Figure 1. Sketch of the flapping caudal fin.

It is interesting to compare the flapping motion under consideration with an undulatory motion to look for possible similarities concerning the existence of a phase velocity also in the present case. By considering sufficiently small values of the maximum pitch angle θ_0 , the flapping motion of the tail given by equation (18) may be approximated as

$$y(x, t) \approx h_0 \sin(2\pi ft) - \theta_0 x \cos(2\pi ft) \quad 0 \leq x \leq l_t \quad (19)$$

where s_f has been confused with the abscissa x . This approximated expression may be assimilated to the one for an undulatory motion of amplitude h_0 with a wavelength $\lambda \gg l_t$

$$\begin{aligned} y(x, t) &= h_0 \sin\left(2\pi ft - \frac{2\pi}{\lambda} x\right) \\ &\approx h_0 \sin(2\pi ft) - \frac{2\pi}{\lambda} h_0 x \cos(2\pi ft) \quad 0 \leq x \leq l_t \end{aligned} \quad (20)$$

and, by equating the coefficients of (19) and (20), we may evaluate the phase velocity of the flapping motion as

$$c = f\lambda \approx 2\pi f \frac{h_0}{\theta_0}. \quad (21)$$

In other words, if $\lambda \gg l_t$, the flapping tail itself may be seen as a small portion of the longer wave whose undulating motion is perceived, instantaneously, as a local oscillation given by the heave and pitch motions.

The above derived equation (21) for the phase velocity associated to the tail reminds in some way the proportional-feathering parameter $\Theta = \theta_0 U_{loc}/2\pi f h_0$, ingeniously suggested by Lighthill [32] to qualify the propulsive performance of flapping foils. It is straightforward to obtain the expression of Θ in this case simply as the ratio between the locomotion velocity U_{loc} and the phase velocity given by equation (21), usually identified as the slip velocity [39].

One of the main parameters characterizing the flapping motion of the caudal fin is the peak-to-peak oscillation amplitude of the trailing edge A_{te} which, for small values of the θ_0 , may be approximated by using the following expression:

$$A_{te} \approx 2 \sqrt{h_0^2 + 2 h_0 l_t \theta_0 \cos(\phi) + l_t^2 \theta_0^2} \quad (22)$$

valid for any value of the phase-lag. In the present case, since the phase angle ϕ is equal to $-\pi/2$, equation (22) reads as

$$A_{te} \approx \sqrt{A_h^2 + 4 l_t^2 \theta_0^2} \quad (23)$$

where the peak-to-peak heave amplitude A_h has been defined as $A_h = 2 h_0$. By combining equations (21) and (23), it follows

$$c \approx 2\pi f l_t \frac{A_h/A_{te}}{\sqrt{1 - (A_h/A_{te})^2}} \quad (24)$$

where it can be appreciated how the phase velocity depends only on the ratio between A_{te} and the maximum excursion of the peduncle A_h . In other words, if A_h/A_{te} is fixed, the phase velocity would be constant no matter the value of A_{te} . From equation (24), it is interesting to note how the phase velocity is rapidly increasing for A_h/A_{te} going to one.

To restrict in a reasonable way the parameter space to be analyzed, we fixed the value of the design trailing edge oscillation amplitude A_{te} that is usually taken to be approximately 0.2 from well-known experimental evidence [40].

3. Results

We consider a fishlike body self-propelled by an oscillating caudal fin in free swimming mode with no viscous resistance. This ideal case is shown to be very useful to understand how the recoil is combined with the prescribed caudal fin motion to obtain the resulting flapping kinematics.

As a first step, the time history of the forward velocity and of the fluid kinetic energy (see equation (10)) for different values of the design parameters in free swimming condition are reported in figures 2(a) and (b), respectively. After an initial transient, the forward velocity reaches a steady-state condition characterized by fluctuations around a mean value classically identified as the locomotion velocity U_{loc} . By looking at both figures 2(a) and (b), we may observe how the kinetic energy transferred to the fluid (see section 2) increases for larger oscillation amplitude of the forward velocity, i.e. for increasing values of the design pitch amplitude θ_0 . At the same time, due to the fixed value of the design parameter A_{te} , a decrease of θ_0 is accompanied by an increase of the heave amplitude h_0 , which may be associated to larger value of the locomotion velocity.

At this point it is instructive to discuss how the phase velocity and the asymptotic locomotion speed are related to the main parameters h_0 and θ_0 .

A simple gait representation is given by figure 3(a) which has been constructed by reporting a few successive configurations of the entire body in free swimming mode to highlight, with their envelope, the wave-like character of the caudal fin motion. We may observe how the tail trajectory follows a sinusoidal path characterized by a wavelength λ obtained with a good approximation as

$$\lambda = \frac{c}{f} \approx 2\pi \frac{h_0}{\theta_0} \quad (25)$$

where the phase velocity c has been evaluated by using equation (21) with the flapping parameters h_0 and θ_0 obtained in free swimming condition. From the same figure and even better from the related animation (see the movie in the supplementary material [online](#)), it appears that the caudal fin motion drives the swimming gait along a traveling wave, while the anterior body seems to have a neutral role with respect to the illustrated motion. More specifically, figure 3(b) reports a comparison between the forward locomotion speed and the estimated phase velocity c both for the case of a swimmer not accounting for any recoil motion, from now on referred to as no-recoil swimmer, and for the case of a fully free swimmer characterized by the same initial design parameters. In both cases the estimated value of the phase velocity, through equation (24) with the proper values of the parameters, is quite close to the actual value of the locomotion speed, though a large difference is observed between the two swimming conditions. The mean power consumption P_m is reported in figure 3(c) to show the different trends with respect to design value of A_h/A_{te} . While P_m is decreasing as A_h/A_{te} goes to one for the free swimmer, the opposite is occurring for the no-recoil swimmer. It follows a markedly better performance in terms of cost of transport when the fish is able to exploit the recoil motions to line up its body to the fluid flowing about, with a resulting more streamlined swimming style. The focus of the paper is on the analysis of the above differences in locomotion speed and expended power which are clearly due to the recoil motions accounted for only in the free mode. A careful investigation on its effects is still not available in the literature for oscillatory free swimming and a further deepening on the subject is certainly due. To this purpose, the adopted impulse model allows for the separation of the recoil in its geometrical, potential and vortical components whose different impact on the tail flapping parameters in free swimming mode are going to be presented below and carefully discussed in the next section.

Figure 4(a) shows the excursion ΔA_h of the peak-to-peak heave amplitude induced by the different recoil motions for all the cases under investigation. Both the geometrical and the potential recoil

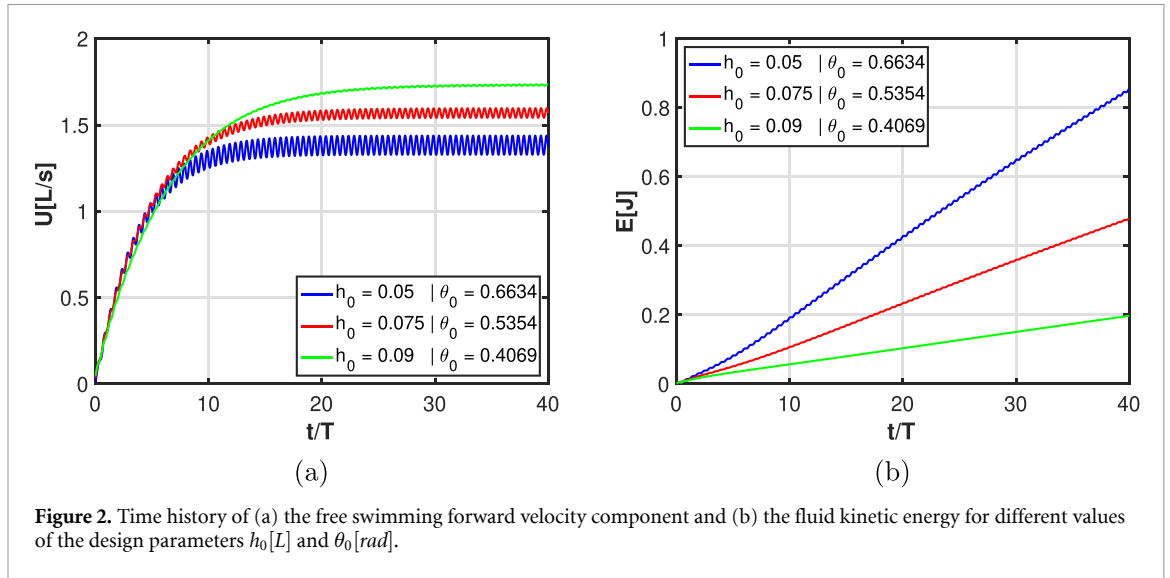


Figure 2. Time history of (a) the free swimming forward velocity component and (b) the fluid kinetic energy for different values of the design parameters h_0 [L] and θ_0 [rad].

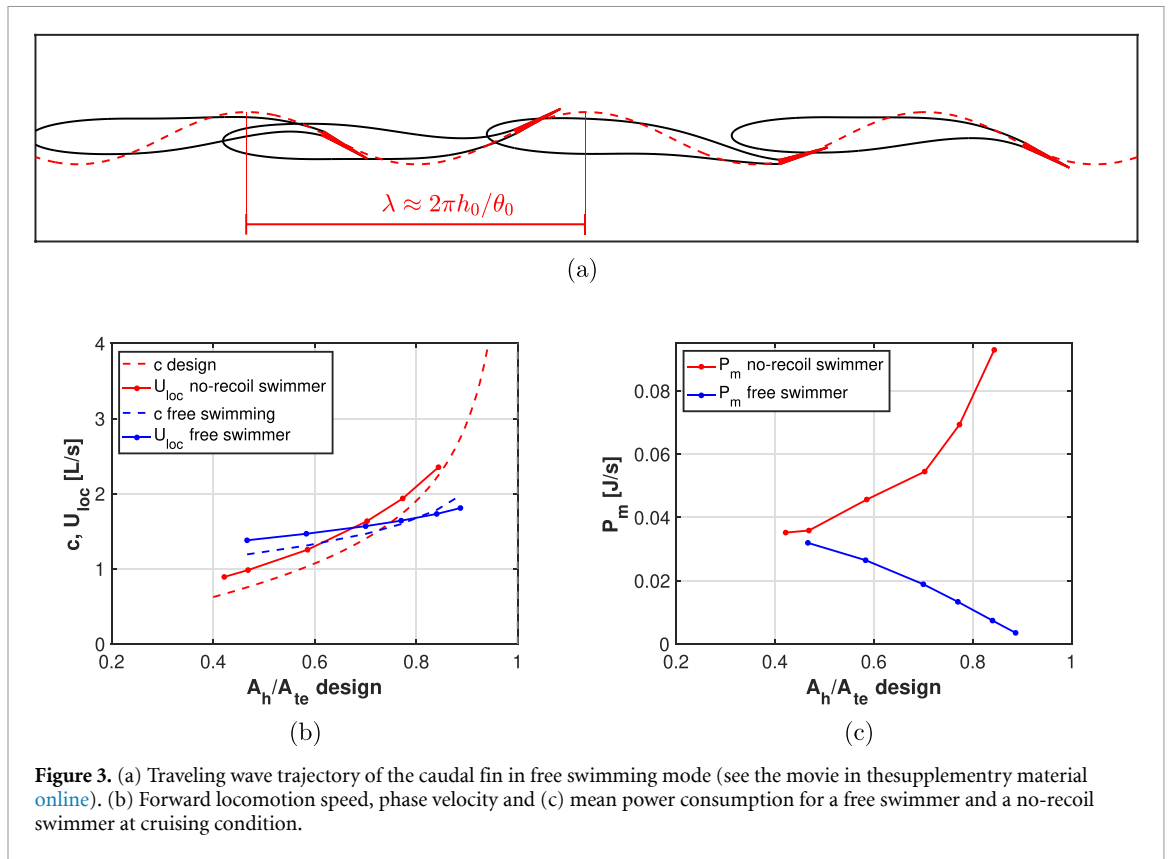
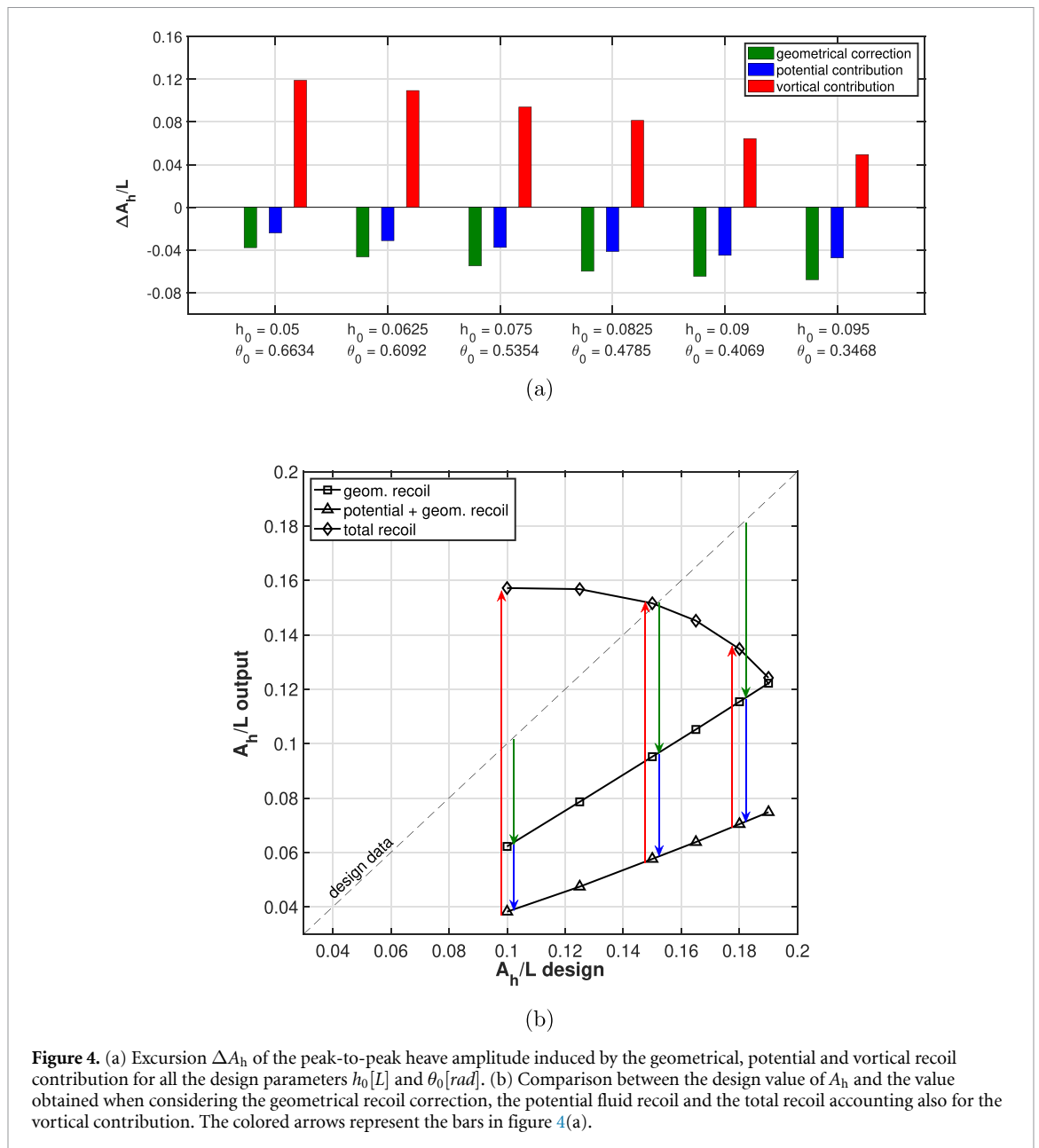


Figure 3. (a) Traveling wave trajectory of the caudal fin in free swimming mode (see the movie in the supplementary material online). (b) Forward locomotion speed, phase velocity and (c) mean power consumption for a free swimmer and a no-recoil swimmer at cruising condition.

contributions are always negative and are increasing in their absolute value for larger design value of h_0 , consequently leading to a reduction of the free swimming peak-to-peak peduncle amplitude A_h . On the other hand, the vortical contribution to ΔA_h given by the vortex shedding in the wake, shows exactly the opposite behaviour by decreasing with the prescribed h_0 , i.e. increasing with θ_0 according to equation (23), and by showing a clear tendency to enhance the heave amplitude A_h , whose large values are commonly associated to a great propulsive capability. The final value of A_h may be obtained by

starting from its design value and summing up all the different contributions as reported in figure 4(b) where the colored arrows are representative of the bars in figure 4(a). By looking at the data obtained in free swimming condition in comparison with the prescribed ones, in some cases we notice an increase while in others a decrease of the heave amplitude, resulting in a quite unclear trend for the variation induced by the total recoil motions. However, by isolating the geometrical, potential and vortical contributions, a monotonic behaviour is clearly obtained for each component. Specifically, the geometrical recoil

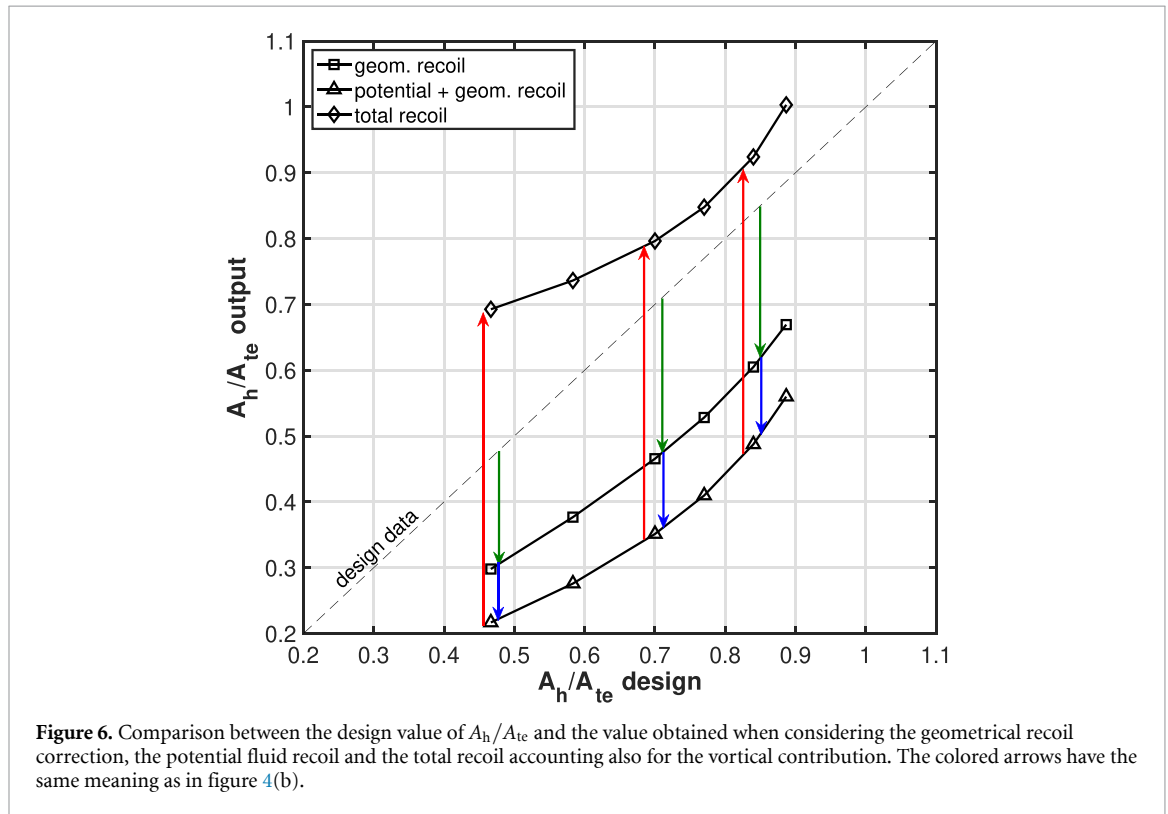
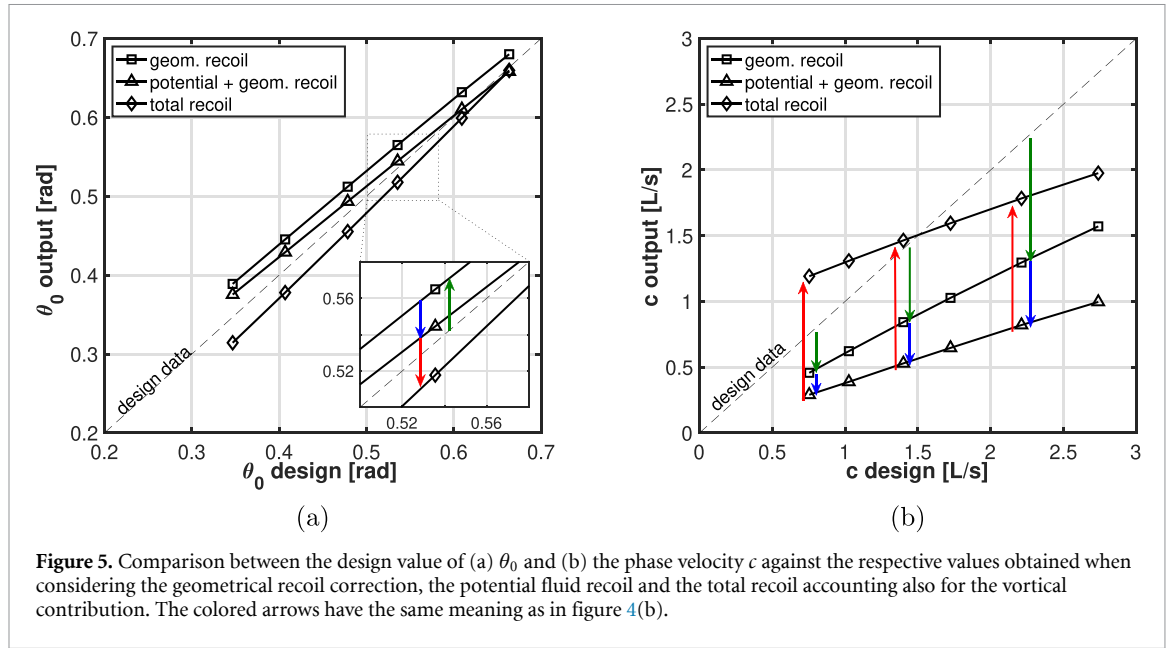


correction is always giving a decrease in the peak-to-peak heave amplitude, followed by a further decrease due to the pure potential flow. The final value of A_h is reached when we consider also the vortical contribution, which always leads to its increase with respect to the potential case.

By adopting the same representation used for A_h (figure 4(b)), we observe how for the pitch angle θ_0 , reported in figure 5(a), the influence of recoil motions seems to be quite negligible. Actually, the final θ_0 values, obtained once the total fluid recoil motions are considered, do not show a significant variation with respect to the design values. Nevertheless, it should be noticed that in this case the geometrical correction is going to increase the value of θ_0 , while both fluid contributions have an opposite effect. The estimated phase velocity c and the ratio

A_h/A_{tc} reported in figures 5(b) and 6 show the same behaviour observed in figure 4(b) for A_h . Namely, the vortical fluid recoil is always contrasting the deterioration generated by the geometrical recoil correction and by the potential fluid recoil to enhance the values of the peak-to-peak values A_h/A_{tc} and of the phase velocity c driving the asymptotic locomotion speed.

By comparing figures 5(b) and 6, it appears that even if the free swimming value of the ratio A_h/A_{tc} is always increasing with respect to its design value, the same is not true for the phase velocity, whose trend follows closely the one observed in figure 4(b) for A_h . For the sake of consistency, this is not conflicting with the increase in the phase velocity with A_h/A_{tc} suggested by equation (24) which is strictly valid for prescribed swimming with a phase lag between the



peduncle heave motion and the pitch of the caudal fin equal to $-\pi/2$, condition which is not usually verified in the free swimming mode under investigation in the present paper.

4. Discussion

As theoretically discussed in section 2, the deformation resulting from the geometrical parameters prescribed in a design procedure, in general, does not satisfy the equilibrium equations in the absence of fluid

interactions as required to guarantee its feasibility in this condition. Figure 7(a) reports an extremely simplified sketch of a flapping fishlike body to attack such a subtle issue, frequently underestimated in the literature. The first frame on the left illustrates the body in its straight and undeformed configuration, while the second one illustrates a deformed one where the body rear-end representative of the tail is flexed by a clockwise angle β . For a fixed anterior body, the rotation of the tail is going to induce a downward motion of the body center of mass CM and a clockwise rotation of the inertia principal axes. However,

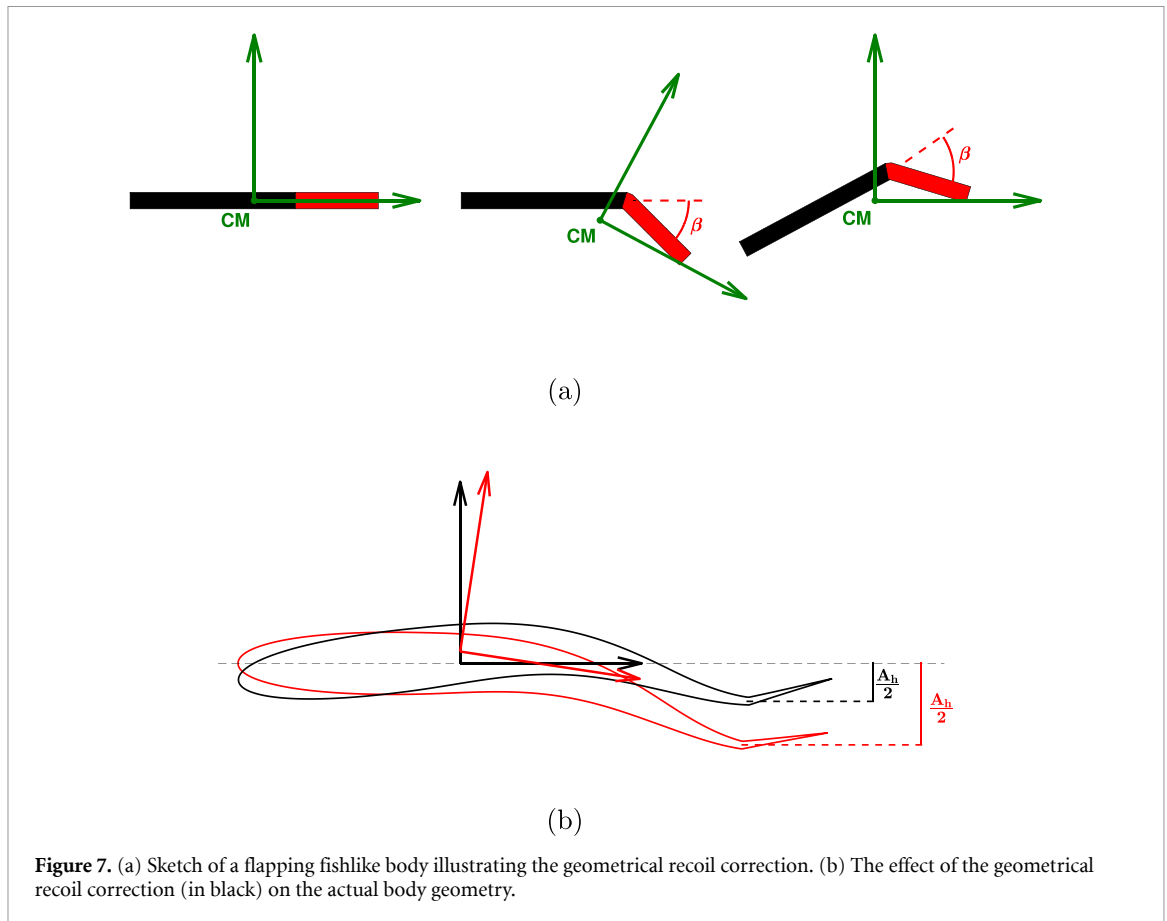


Figure 7. (a) Sketch of a flapping fishlike body illustrating the geometrical recoil correction. (b) The effect of the geometrical recoil correction (in black) on the actual body geometry.

for an isolated body, neither the translation of its center of mass nor the rotation of its principal axes are allowed since no external actions are applied. In this condition, the geometrical recoil correction is the motion required to make this configuration feasible, i.e. the motion required to go from the central frame in figure 7(a) to the last frame on the right, where the center of mass and the principal axes perfectly match the ones for the undeformed configuration. In this way, any spurious rigid motion introduced in the design procedure is annihilated by the geometrical recoil, whose impact on the actual body geometry is illustrated by figure 7(b) that gives a qualitative insight on its overall effects on the prescribed deformation. The results reported in the previous section show how the geometrical correction presents a general tendency to reduce all the relevant data but the pitch angle θ_0 , whose variation is very small. As a consequence, the large reduction of the peduncle heave amplitude A_h leads to a smaller value of the asymptotic phase velocity c , hence to a lower performance in terms of the related locomotion speed. It follows that the geometrical recoil correction is definitely negative for the fish propulsive capability and it should be minimized, at least, for fully constrained motions [19, 20] to avoid such an evident deterioration of the performance. This last consideration is probably the reason for the bad reputation erroneously gained

in the past by the recoil with regard to swimming performance. Actually, the concept of recoil correction was initially introduced by Lighthill as a unique rigid motion, not distinguishing between the correction due to the interaction with the surrounding fluid and the geometrical one, which led subsequently to contradictory opinions on the subject. To this regard, a typical consideration is that some fish species have evolved deep and heavy head to counterbalance the rapid motions of the light caudal fin so to reduce lateral and angular oscillations about the center of mass to avoid performance deterioration, which is consistent, in the framework of our model, with the results reported in the previous section for the geometrical recoil.

Going now to the fluid recoil contributions, as illustrated in the section 2, the linearity of the present model allows for the separation of the potential-induced velocity components ($U_\phi, V_\phi, \Omega_\phi$) from the vortical-induced velocity components (U_v, V_v, Ω_v) which, once combined, give the total fishlike body kinematics. This particular property of the model led to the results reported in figures 4–6 which clearly show how, even though the potential recoil gives another negative effect, the vortical recoil contribution is always leading to a consistent improvement of the flapping parameters. The opposite behaviour of the vortical contribution with respect

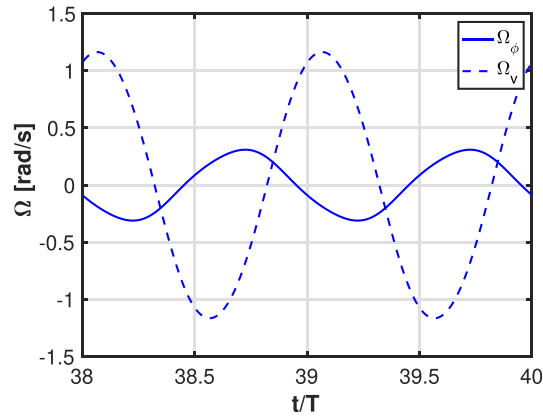


Figure 8. Comparison between the time history of the potential, Ω_ϕ , and vortical, Ω_v , contributions to the body angular velocity.

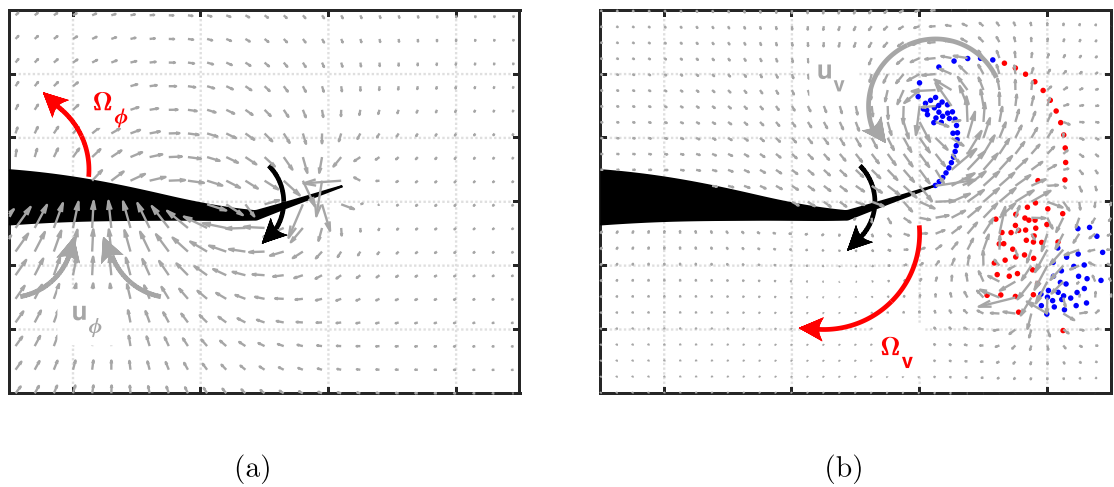


Figure 9. Flow field sketches for (a) the potential fluid recoil and (b) the vortical fluid recoil.

to the potential one is observable from the comparison between the time history of the potential-induced angular velocity Ω_ϕ with the vortical-induced angular velocity Ω_v reported in figure 8 for one sample case. The potential contribution Ω_ϕ has an opposite phase with respect to the vortical one Ω_v . This behaviour is perfectly consistent with the physical meaning of the two contributions related to the added mass and to the vortex shedding, respectively. The sample flow fields reported in figure 9, inspired by previous analyses [41, 42], may give a simple idea to understand their counteracting role. As illustrated in figure 9(a), the potential acyclic field \mathbf{u}_ϕ generated by the caudal fin downstroke leads to a counterclockwise angular velocity Ω_ϕ in the opposite direction with respect to tail motion. It follows that the potential recoil contribution, increasing with the body deformation (see figures 4–6), tends to counterbalance and to attenuate the tail oscillation. On the other hand, the vortical field reported in figure 9(b) shows an opposite behaviour since the fluid vortical velocity \mathbf{u}_v induced by the vortex cluster just released

by the body is going to enhance the tail motion via the angular recoil velocity Ω_v , as it may easily result from figure 4(a).

As a general comment, it is worth to underline the tendency of the fluid recoil to enhance the heave amplitude up to a value strictly comparable with the trailing edge excursion A_{te} as shown by the increase of the ratio A_h/A_{te} which represents the fraction of the trailing edge amplitude due to the heave motion of the peduncle. The more A_h/A_{te} approaches unity, the more the caudal fin is flat at its maximum lateral position, so to lay, together with the anterior body, on the sinusoidal trajectory and to obtain a good swimming performance [9, 43]. Actually, the relationship between a high swimming performance and a flat tail excursion was already envisaged in the early sixties by Lighthill [15] who suggested to annihilate the slope of the midline amplitude modulation to maximize the swimming efficiency. Interestingly for the no-recoil swimmer, since the body is not able to align with the flow, the expended energy keeps increasing with A_h/A_{te} as shown in figure 3(c).

5. Concluding remarks

The different style of swimming proper of different fish species brought, in the past, to several specific approximations, which in most cases are not anymore strictly required [44]. For instance, oscillatory swimming, classically investigated in axial motion to look for the best propulsive efficiency of the caudal fin, should be analyzed by considering the free mode of the whole body, as commonly done for undulatory swimming. In fact, the free self-propulsion reveals the importance of the recoil rigid motions, given by the fluid interaction, which are essential to guarantee the overall equilibrium and may drastically modify the kinematics of the caudal fin with respect to the prescribed one, to finally obtain a better swimming performance. The recoil reaction and the locomotion speed are obtained here by a simple impulse model able to highlight the added mass and the released vorticity contributions, together with their coupling terms which are especially important in transient conditions [45]. This model allows to understand the capability of the potential terms to attenuate the recoil reaction continuously forced by the vortex shedding which is directly related to the wasted energy. Since the input deformation prescribed in a design procedure usually is not satisfying the equilibrium equations to guarantee null rigid motions of the body in the absence of fluid interaction, the induced spurious rigid displacements are removed by a geometrical recoil correction. The direct application of the impulse model to such corrected shape deformation helps the physical interpretation of the results since it provides a more clear pattern from the input to the output values of the caudal fin parameters. In fact, by combining the fluid recoil with both heave and pitch motions modified by the geometrical recoil, the actual features of the caudal fin in the inertial frame are identified together with the associated phase velocity which drives the locomotion speed in inviscid flows. In a few words, the illustrated simple model may give helpful suggestions to figure out the free motion of a biomimetic body in water and to select a deformation able to generate the desired swimming performance for biomimetic technological means.

Data availability statement

All data that support the findings of this study are included within the article (and any supplementary files).

Acknowledgments

This research was founded by Sapienza University of Rome through a research grant to G G and D P

Regione Lazio is also acknowledged for the support of L P PhD fellowship.

Appendix. Anterior body deformation

For the prescribed deformation of the anterior body, we followed a path similar to the one suggested by Li et al [38] for a pure oscillation up the peduncle, but we consider a proper undulatory motion with wavelength λ to better represent the shape deformations observed in real fish and to better fit the flapping motion of the caudal fin. In details, the first third of the anterior body midline is fixed and the remaining rear-end of length $l_r = l_b - 1/3$ is divided into N segments of length l_j . For a given peduncle oscillation amplitude h_0 , the lateral motion $y_i(t)$ of the left edge of each segment is defined as

$$\begin{cases} y_1(s_1, t) = 0 \\ y_i(s_i, t) = h_i \sin\left(2\pi ft - \frac{2\pi}{\lambda} s_i\right) & i = 2, \dots, N \\ y_p(t) = h_p \sin\left(2\pi ft - \frac{2\pi}{\lambda} l_r\right) & \text{for the peduncle} \end{cases} \quad (.1)$$

where the coefficients h_i is the maximum lateral displacement of the i th segment and s_i is a curvilinear abscissa going from 0 to 1, i.e. from the first third of the body to the peduncle. The coefficients h_i and the instantaneous inclination of each segment Ψ_i may be obtained as follows

$$\begin{cases} h_1 = 0 \\ h_i = h_0 \left(\frac{\sum_{j=1}^{i-1} l_j}{l_r}\right)^2 & i = 2, \dots, N \end{cases} \quad (.2)$$

$$\begin{cases} \Psi_i(s_i, t) = \arcsin \frac{y_{i+1}(s_{i+1}, t) - y_i(s_i, t)}{l_i} & i = 1, \dots, N-1 \\ \Psi_N(s_N, t) = \arcsin \frac{y_p(t) - y_N(s_N, t)}{l_N} \end{cases} \quad (.3)$$

ORCID iDs

D Paniccia  <https://orcid.org/0000-0002-1154-2783>

G Graziani  <https://orcid.org/0000-0002-7522-6755>

References

- [1] Garrick I E 1936 Propulsion of a flapping and oscillating airfoil *National Advisory Committee for Aeronautics: Report (NACA)* vol 567
- [2] Jones K and Platzer M 1997 Numerical computation of flapping-wing propulsion and power extraction *AIAA Paper* vol 97 p 0826

- [3] Anderson J M, Streitlien K, Barrett D S and Triantafyllou M S 1998 Oscillating foils of high propulsive efficiency *J. Fluid Mech.* **360** 41–72
- [4] Young J and Lai J C S 2007 Mechanisms influencing the efficiency of oscillating airfoil propulsion *AIAA J.* **45** 1695–702
- [5] Floryan D, Van Buren T, Rowley C W and Smits A J 2017 Scaling the propulsive performance of heaving and pitching foils *J. Fluid Mech.* **822** 386–97
- [6] Fernandez-Feria R 2017 Note on optimum propulsion of heaving and pitching airfoils from linear potential theory *J. Fluid Mech.* **826** 781–96
- [7] Akoz E and Moored K W 2018 Unsteady propulsion by an intermittent swimming gait *J. Fluid Mech.* **834** 149–72
- [8] Akoz E, Han P, Liu G, Dong H and Moored K W 2019 Large-amplitude intermittent swimming in viscous and inviscid flows *AIAA J.* **57** 1–8
- [9] Paniccia D, Padovani L, Graziani G and Piva R 2021 The performance of a flapping foil for a self-propelled fishlike body *Sci. Rep.* **11** 22297
- [10] Li G, Liu H, Muller U K, Voeselek C J and van Leeuwen J L 2021 Fishes regulate tail-beat kinematics to minimize speed-specific cost of transport *Proc. R. Soc. B* **288** 20211601
- [11] Carling J, Williams T L and Bowtell G 1998 Self-propelled anguilliform swimming simultaneous solution of the two-dimensional navier-stokes equations and newtons laws of motion *J. Exp. Biol.* **201** 3143–66
- [12] Kern S and Koumoutsakos P 2006 Simulations of optimized anguilliform swimming *J. Exp. Biol.* **209** 4841–57
- [13] Yang Y, Wu G H, Yu Y-L and Tong B G 2008 Two-dimensional self-propelled fish motion in medium an integrated method for deforming body dynamics and unsteady fluid dynamics *Chin. Phys. Lett.* **25** 597–600
- [14] Borazjani I and Sotiropoulos F 2010 On the role of form and kinematics on the hydrodynamics of self-propelled body-caudal fin swimming *J. Exp. Biol.* **213** 89–107
- [15] Lighthill J 1960 Note on the swimming of slender fish *J. Fluid Mech.* **9** 305–17
- [16] Li G, Muller U K, van Leeuwen J L and Liu H 2012 Body dynamics and hydrodynamics of swimming fish larvae: a computational study *J. Exp. Biol.* **215** 4015–33
- [17] Reid D A P, Hildenbrandt H, Padding J T and Hemelrijk C K 2012 Fluid dynamics of moving fish in a two-dimensional multiparticle collision dynamics model *Phys. Rev. E* **85** 021901
- [18] Maertens A P, Gao A and Triantafyllou M S 2017 Optimal undulatory swimming for single fish-like body and for pair of interacting swimmers *J. Fluid Mech.* **813** 301–45
- [19] Paniccia D, Graziani G, Lugni C and Piva R 2021 The relevance of recoil and free swimming in aquatic locomotion *J. Fluids Struct.* **103** 103290
- [20] Sohn S 2021 A computational model of the swimming dynamics of a fish-like body in two dimensions *Phys. Fluids* **33** 121902
- [21] Lighthill J 1971 Large-amplitude elongated body theory of fish locomotion *Proc. R. Soc. B* **179** 126–38
- [22] Noca F 1997 On the evaluation of time-dependent fluid dynamic forces on bluff bodies *PhD Thesis* California Institute of Technology
- [23] Graziani G and Bassanini P 2002 Unsteady viscous flows about bodies: Vorticity release and forces *Meccanica* **37** 283–303
- [24] Wu J Z, Ma H Y and Zhou M D 2015 *Vortical Flows* (Berlin: Springer)
- [25] Paniccia D, Graziani G, Lugni C and Piva R 2021 On the role of added mass and vorticity release for self propelled aquatic locomotion *J. Fluid Mech.* **918** A45
- [26] Bhalla A P S, Bale R, Griffith B E and Patankar N A 2013 A unified mathematical framework and an adaptive numerical method for fluid-structure interaction with rigid deforming and elastic bodies *J. Comput. Phys.* **250** 446–76
- [27] Singh K and Pedley T J 2008 The hydrodynamics of flexible-body manoeuvres in swimming fish *Physica D* **237** 2234–9
- [28] Kansa E 2009 Swimming due to transverse shape deformations *J. Fluid Mech.* **631** 127–48
- [29] Saffman P G 1967 The self-propulsion of a deformable body in a perfect fluid *J. Fluid Mech.* **28** 385
- [30] Lamb H 1975 *Hydrodynamics* 6th edn (Cambridge: Cambridge University Press)
- [31] Borazjani I and Sotiropoulos F 2008 Numerical investigation of the hydrodynamics of carangiform swimming in the transitional and inertial flow regimes *J. Exp. Biol.* **211** 1541–58
- [32] Lighthill J 1970 Aquatic animal propulsion of high hydromechanical efficiency *J. Fluid Mech.* **44** 265–301
- [33] Hess J L and Smith A M O 1967 Calculation of potential flow about arbitrary bodies *Prog. Aerosp. Sci.* **8** 1–138
- [34] Basu B C and Hancock G J 1978 The unsteady motion of a two-dimensional aerofoil in incompressible inviscid flow *J. Fluid Mech.* **87** 159–78
- [35] Jones K D, Dohring C M and Platzer M F 1998 Experimental and computational investigation of the knoller-betz effect *AIAA J.* **36** 1240–6
- [36] Young J 2005 Numerical simulation of the unsteady aerodynamics of flapping airfoils *PhD Thesis* The University of New South Wales
- [37] Platzer M F, Jones K D, Young J and Lai J C S 2008 Flapping wing aerodynamics: progress and challenges *AIAA J.* **46** 2136–49
- [38] Li N, Liu X and Su Y 2017 Numerical study on the hydrodynamics of thunniform bio-inspired swimming under self-propulsion *PLoS One* **12** e0174740
- [39] Wu T Y 2011 Fish swimming and bird/insect flight *Annu. Rev. Fluid Mech.* **43** 25–58
- [40] Bainbridge R 1958 The speed of swimming of fish as related to size and to the frequency and amplitude of the tail beat *J. Exp. Biol.* **35** 109–33
- [41] Pollard B and Tallapragada P 2019 Passive appendages improve the maneuverability of fishlike robots *IEEE/ASME Trans. Mechatronics* **24** 1586–96
- [42] Hang H, Heydari S, Costello J H and Kansa E 2022 Active tail flexion in concert with passive hydrodynamic forces improves swimming speed and efficiency *J. Fluid Mech.* **932** A35
- [43] Ayancik F, Fish F and Moored K 2020 Three-dimensional scaling laws of cetacean propulsion characterize the hydrodynamic interplay of flukes' shape and kinematics *J. R. Soc. Interface* **17** 20190655
- [44] Di Santo V, Goerig E, Wainwright D, Akanyeti O, Liao J, Castro-Santos T and Lauder G 2021 Convergence of undulatory swimming kinematics across a diversity of fishes *Proc. Natl Acad. Sci.* **118** e2113206118
- [45] Paniccia D, Graziani G, Lugni C and Piva R 2022 The fish ability to accelerate and suddenly turn in fast maneuvers *Sci. Rep.* **12** 4946